IEEE Access
Multidisciplinary | Rapid Review | Open Access Journal

Received March 2, 2020, accepted March 11, 2020, date of publication March 19, 2020, date of current version March 31, 2020.

Digital Object Identifier 10.1109/ACCESS.2020.2982036

Ultra-Wideband MIMO Antenna System With High Element-Isolation for 5G Smartphone Application

XIAO-TING YUAN[1], WEI HE[2], KAI-DONG HONG[1], CHONG-ZHI HAN[1], ZHE CHEN[1], (Member, IEEE), AND TAO YUAN[1,3], (Member, IEEE)

[1]Guangdong Provincial Mobile Terminal Microwave and Millimeter-Wave Antenna Engineering Research Center, College of Electronics and Information Engineering, Shenzhen University, Shenzhen 518060, China
[2]China Academy of Information and Communications Technology (CAICT), Beijing 100876, China
[3]ATR National Key Laboratory of Defense Technology, College of Electronics and Information Engineering, Shenzhen University, Shenzhen 518060, China

Corresponding author: Zhe Chen (cz317858026@163.com)

This work was supported in part by the National Natural Science Foundation of China under Grant 61801300, in part by the Fundamental Research Program of Shenzhen Science and Technology Innovation Committee, China, under Project No. JCYJ20180305124721920 and in part by the Shenzhen Innovation and Entrepreneurship Program for Overseas High-Level Talents, China, under Group Project No. KQTD20180412181337494.

ABSTRACT In this paper, we presented an ultra-wideband multiple-input multiple-output (MIMO) antenna system with high element-isolation for the application in 5G metal-frame smartphones. We proposed T-shaped and C-shaped slots on the metal frame generating four resonances to enhance the bandwidth. What's more, we introduce modified H-shaped slots between each antenna-element to improve the element-isolation of MIMO antenna system. As a result, the MIMO antenna system has a wide bandwidth of 58% ranging from 3.3 to 6 GHz and the element-isolation is over 18 dB crossing the effective frequency band. Thanks to the decent element-isolation, the envelope correlation coefficient (ECC) between each antenna-element is below 0.05 providing a reliable anti-interference for the MIMO antenna system. In addition, the measured radiation efficiencies of the MIMO antenna system are higher than 40%. At last, we analyze the effects caused by user's hands and head to guarantee the robustness of the MIMO antenna system in practical applications.

INDEX TERMS 5G communication, sub-6 GHz, ultra-wideband, high isolation, metal frame.

I. INTRODUCTION

With the commercialization of the fifth generation (5G) mobile communication, high data rate communication and intelligent wireless services is approaching [1], [2]. However, the 5G technology brings challenges such as the requirement of the high throughput of the wireless system. To solve this problem, wide bandwidth and MIMO technologies are indispensable to enhance the channel capacity and spectrum efficiency by exploiting multipath property without increasing the input power [3]. Compared to the conventional 3G/4G mobile phone antenna system, 5G mobile phone prefers MIMO antenna system such as 8×8 or even 10×10 MIMO antenna systems [4], [5]. Furthermore, the MIMO system should possess the characteristics of broadband and high element-isolation to contribute promising performance. According to the World Radio Communication Conference in 2015, different countries and operators have adopted various frequency bands for 5G communication. For example, LTE band 42 (3400–3600 MHz) and LTE band 43 (3600–3800 MHz) have been approved by European Union. Japan and China have authorized 3600-4200/4400-4900 MHz and 3300-3600/4800-5000 MHz, respectively. Additionally, LTE band 46 (5150–5925 MHz) would join the family of 5G frequency band soon. To cover these frequency bands, broadband is a key feature for the MIMO antenna system in 5G application. To our best of knowledge, the mutual coupling between each antenna-element would deteriorate the throughput of the MIMO antenna system. Consequently, how to improve the element-isolation is a challenge to design a reliable MIMO antenna system. What's more, how to integrate such a MIMO antenna system into a space-limited smartphone with metal frame is quite difficult.

Several MIMO antenna systems for smartphones have been reported in recent years [6]–[31], demonstrating its superiority in transmission rate and channel capacity. A few

The associate editor coordinating the review of this manuscript and approving it for publication was Lu Guo.

reported MIMO antenna designs could cover single band in sub-6GHz spectrum [6]–[20]. To improve the throughput, some MIMO antenna designs have enhanced their impedance bandwidth to involve more frequency bands in sub-6GHz spectrum [21]–[31]. In these designs, MIMO antenna systems in smartphone with metal frame have been presented [19], [20], [30], [31]. However, the designs in [19], [20], [30] had to endure the narrow bandwidth limitation due to the cruel electromagnetic environment. Only the MIMO antenna system in [31] has overcome this dilemma and covered an ultra-wide frequency band in sub-6GHz spectrum. In addition to the bandwidth, we need to consider the effect of element-isolation on the throughput of the MIMO antenna system.

To our best of knowledge, decoupling technique is an effective method to raise the isolation between each antenna-element. Many decoupling techniques have been adopted to address the isolation problem. For example, the spatial diversity and polarization diversity have been utilized to increase the isolation in the device with large space between each antenna [32]–[35], [42]. [43]. Electromagnetic band gap (EBG) structure [36], frequency selective surface [37], [38] and resonators or hybrid resonators [39]–[41] have been employed to mitigate the mutual coupling in the 2 × 2 MIMO system. In addition, neutralization line [8], [9], [24] is effective in isolation enhancement within narrow frequency band. In reference [8], an inverted-I ground slot has been introduced between the antenna-elements with an excellent element-isolation better than 15 dB. Inspired by the decoupling structure in [8], we initiated a modified H-shaped slot between the antenna-elements and increased the element-isolation to 18 dB.

In this paper, we presented an ultra-wideband MIMO antenna system with high element-isolation for the application in 5G metal-frame smartphones. Unlike other designs suffered from the restricted radiation environment caused by the metal-frame, we etched slots on the metal-frame to explore novel radiation method in the space-limited smartphone MIMO antenna design. What's more, we proposed a modified H-shaped slot to improve the element isolation of the MIMO antenna system. As a result, the MIMO antenna system has an ultra-wide bandwidth of 58% and the in-band element-isolation is over 18 dB, which can cover most of the frequency bands in sub-6GHz spectrum. Compared to the state-of-the-art in this area as in table 1, the proposed MIMO antenna system has a superior performance.

II. MIMO ANTENNA SYSTEM

The geometry of the proposed MIMO antenna system for the 5G smartphone application is shown in Fig. 1. The size of the ground is 150 × 75 mm^2 and the thickness of the smartphone is 7 mm. In the design, we employed the FR4 substrate with a thickness of 0.8 mm (relative permittivity 4.4 and loss tangent 0.02) to build the body of the smartphone. For radiation element, we used copper (conductivity 5.8 × 10^7S/m). The conductivity of copper is very stable and it has little effect on impedance matching.

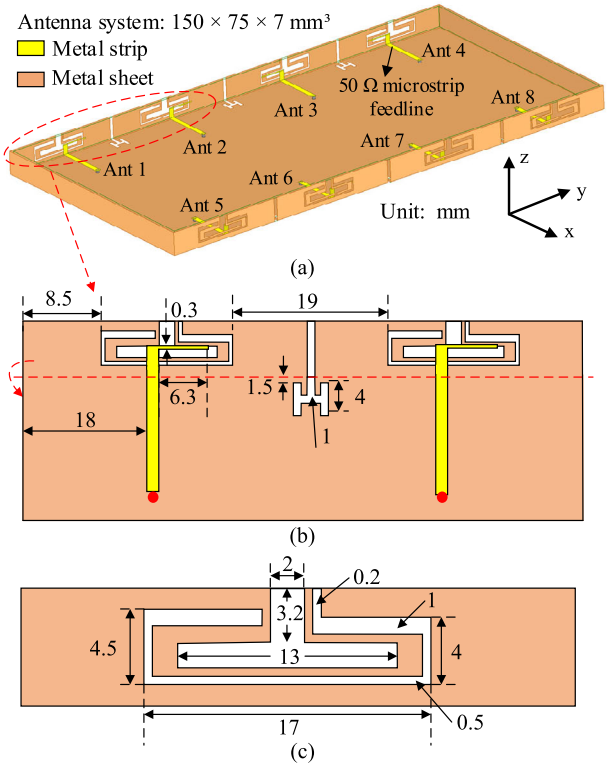

FIGURE 1. Geometry and detailed dimensions of the proposed MIMO antenna system. (a) Overall view, (b) inverted L-shaped micro-strip line and decoupling element, (c) antenna-element.

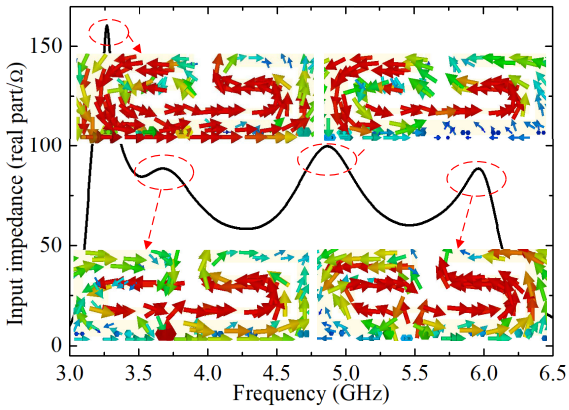

FIGURE 2. Surface current distributions of four resonances.

A. ANTENNA-ELEMENT

An ultra-wideband antenna-element with a size of 17 × 5.7 mm^2 is shown in Fig. 1(c). We carved T- and C-shaped slots on the metal frame and used an inverted L-shaped micro-strip line to couple energy to the slots, thus exciting four resonances to merge into an ultra-wide impedance bandwidth. The surface current distributions of four resonances are shown in Fig. 2. Clearly, the surface current of the first resonance mainly distributes along the C-shaped slot. The surface currents of the second and fourth resonances mainly concentrate in T-shaped slot. However, the second resonance works in its loop mode while the fourth

TABLE 1. Performance comparison with previous published literatures.

Reference	Total size (eight-element)	Metal frame	Decoupling method	Effective bandwidth (GHz)	Isolation (dB)	Total efficiency (%)	ECC
Proposed	150×75×7mm^3	With	Ground slot	3.3-6.0 (-6dB)	>18	40-90	<0.05
[8]	124×74×6mm^3	Without	Ground slot	3.3-3.6 (-6dB)	>15	45-60	<0.15
[12]	150×80×0.8mm^3	Without	No	3.4-3.6 (-6dB)	>17.5	62-76	<0.05
[13]	150×75×0.8mm^3	Without	Polarization orthogonal	3.3-3.8 (-6dB)	>15	60-70	<0.05
[15]	150×75×8mm^3	Without	Polarization orthogonal	3.4-3.6 (-6dB)	>17	49-72.9	<0.1
[19]	145×75×6mm^3	With	No	3.4-3.6 (-6dB)	>15	42-73	<0.16
[20]	150×75×7mm^3	With	No	3.4-3.6 (-6dB)	>12.7	35.2-64.7	<0.13
[24]	150×75×7mm^3	Without	Neutralization line	3.4-3.6 4.8-5.1 (-6dB)	>11.5	40-85	<0.08
[25]	140×70×1mm^3	Without	No	3.4-3.6 5.51-5.93 (-6dB)	>11.2	51-80	<0.08
[28]	150×75×7mm^3	Without	Multi-slot	3.4-3.8 4.8-5.0 (-6dB)	>15.5	40-85	<0.07
[29]	150×75×6.8mm^3	Without	No	3.3-5.0 (-6dB)	>14.7	46-80	<0.05
[31]	150×75×6mm^3	With	No	3.3-6.0 (-6dB)	>11	40-71	<0.1

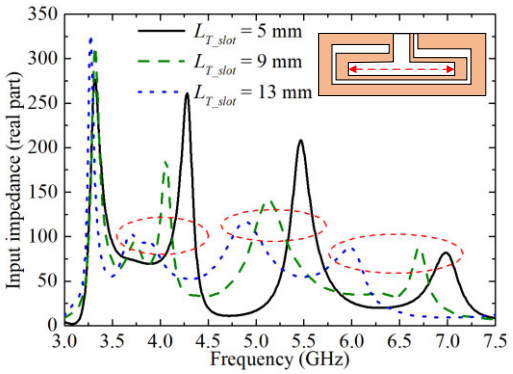

FIGURE 3. Simulated input impedance of antenna-element with effects of the length of T-shaped slot.

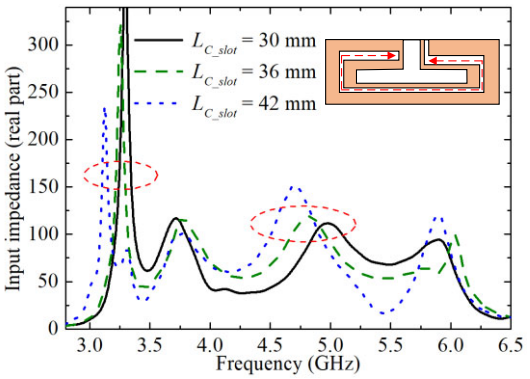

FIGURE 4. Simulated input impedance of antenna-element with effects of the length of C-shaped slot.

resonance operates as a slot mode. The surface current of the third resonance can be found in both C- and T-shaped slot. Consequently, we can say the third resonance is from the coupling between C- and T-shaped slots. To further verify this conclusion, we try to analyze the resonant mechanism by adjusting the electrical length of the T- and C-shaped slots. In Fig. 3, we decrease the length of T-shaped slot and retain the length of C-shaped slot unchanged. We find that the second, third and fourth resonances shift toward higher frequency while the first resonance stays constant. On the contrary, we increase the length of C-shaped slot and maintain the length of T-shaped slot unaltered in Fig. 4. Clearly, the first and third resonances move to lower frequency while the second and the fourth resonances remain unchanged. We can conclude that, the second and forth resonances come from the T-shaped slot, the first resonance is driven by the C-shaped slot and the third resonance is born from the coupling between the T- and C-shaped slots. This conclusion is consistent with the conclusion drawn from surface current distribution. Our goal is to obtain an ultra-wide impedance bandwidth with these four resonances, therefore, we optimize the dimensions of the T- and C-shaped slots and the L-shaped feeding line. The optimal dimensions are shown in Fig. 1(b) and (c). At last, the proposed antenna-element can support an ultra-wideband ranging from 3.3 to 6.0 GHz with reflection coefficient lower than −6 dB (3:1 voltage standing-wave ratio) in Fig. 5.

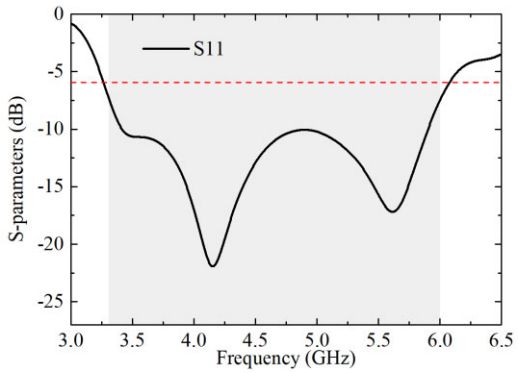

FIGURE 5. Simulate reflection coefficient of antenna-element.

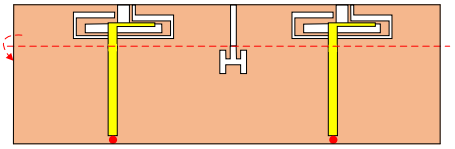

FIGURE 6. The decoupling structure proposed in this paper.

In order to support the high transmission rate in 5G mobile communication, an 8 × 8 MIMO system is arranged based on the antenna-element. The arrangement of the MIMO system is symmetrical and normal shown in Fig. 1(a). The distance between Ant 1 and 2, Ant 2 and 3 is 19 mm and 25 mm, respectively. The space from Ant1 to the edge of the phone is 8.5 mm. As a result, the isolation between antenna-elements is not good. To improve the element-isolation of the MIMO system, we introduced a new decoupling structure.

B. DECOUPLING ELEMENT

To enhance isolation between each two antenna elements, we have tried a lot of decoupling methods. We find that few methods are effective in our design because they cannot constrain the surface current on metal frame. In our design, the coupling between two antenna elements is mainly caused by the surface current on the metal frame. Then, we separated the two antenna elements with a slot etched on the metal frame and employed an H-shaped resonator to constrain the surface current as in Fig. 6. Although this structure increases the antenna clearance area, it can improve the element-isolation in a wideband effectively. For the antenna system with high-isolation requirement but less clearance-limitation this method is recommended. For the antenna system with limited clearance but less isolation requirement, our design without decoupling element can also satisfy the demand.

To verify the mechanism of decoupling element, the surface current distributions without and with decoupling structure are shown in Fig. 7. Compared the surface current distribution between Figs. 7 (a) and (b), we can say that the proposed decoupling element effectively prevents the surface current flowing from Ant1 to Ant2 when Ant1 is excited and Ant2 is terminated with a 50Ω-load. Then we compared the

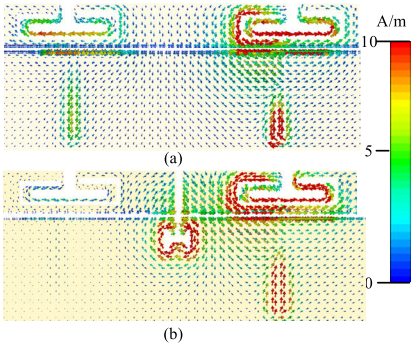

FIGURE 7. Surface current distributions (a) without decoupling structure and (b) with decoupling structure of Ant 1 and 2.

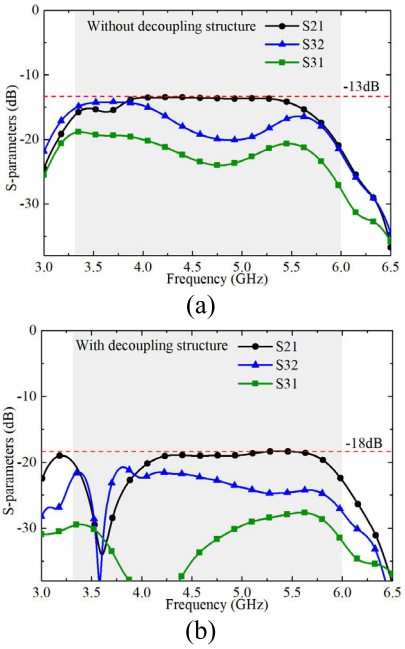

FIGURE 8. Transmission coefficients between any couple of Ant1, 2 and 3 with/without decoupling structure.

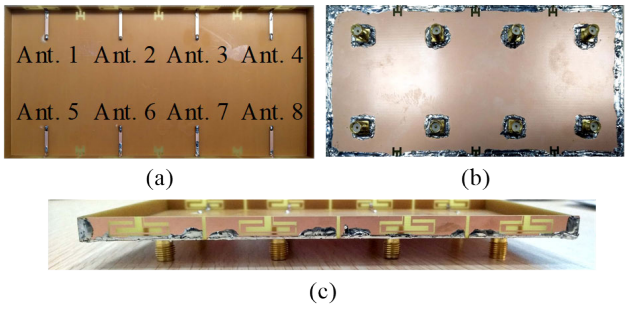

FIGURE 9. Photographs of the fabricated MIMO antenna system. (a) Front view. (b) Back view. (c) Side view.

transmission coefficients between any couple of Ant 1, 2 and 3 in the situation of with and without decoupling element as in Figs. 8. Clearly, the level of element-isolation is improved to more than 18 dB with the decoupling structure, which is quite competitive to the state-of-the-art in this area.

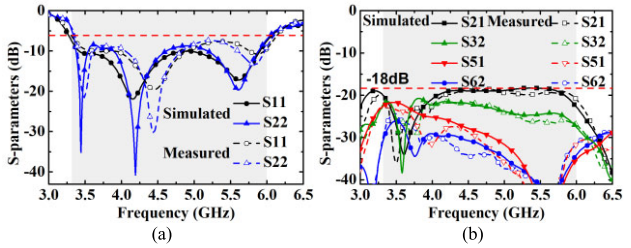

FIGURE 10. Simulated and measured (a) reflection coefficients and (b) transmission coefficients of MIMO antenna system.

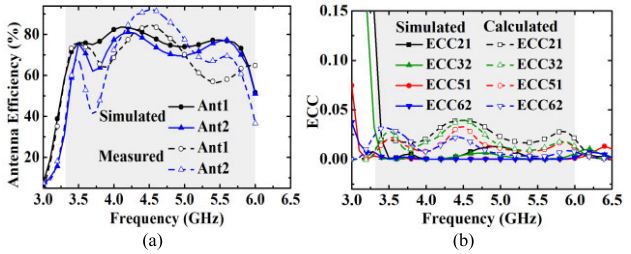

FIGURE 11. Simulated and measured (a) antenna efficiencies and (b) ECCs between some adjacent antenna-element.

III. RESULTS AND DISCUSSION

A. S-PARAMETERS AND EFFICIENCY

We fabricated the proposed MIMO antenna system with the optimal dimensions and measured it in our lab. The photograph of the proposed MIMO antenna system in a metal frame smartphone is shown in Fig. 9. There are eight SMA connectors underground to feed each antenna element for the MIMO antenna system. Owning to the centrosymmetric structure of the MIMO antenna system, we analyze the simulated and measured results for a part of antenna-elements for brevity.

In Fig. 10(a), the simulated and measured reflection coefficients show a good agreement. The −6 dB bandwidth can cover 3.3-6.0 GHz, containing most frequency bands in sub-6GHz spectrum. In Fig. 10(b), we present the transmission coefficients between port 1&2, 2&3, 1&5 and 2&6 because they are adjacent to each other and the couplings between them are stronger than other pairs. The simulation and measurement agree well and the level of element-isolation is more than 18 dB across the target frequency band. In Fig. 11(a), the measured radiation efficiencies are lower than that in the simulation at low and high frequency bands while the situation is opposite at the middle frequency band. It is caused by the reason that the loss tangent of the FR4 substrate is inhomogeneous in measurement across the wide frequency band. The efficiency dip at 3.75 GHz is caused by the insufficient radiation of the current at this frequency. In Fig. 12, we compared the current distribution around the decoupling-slot at different frequencies. Obviously, the magnitude of the current distribution around the decoupling-slot at 3.75 GHz is stronger than that at 4 GHz, which means less energy is radiated through the antenna element at 3.75 GHz. As a result, there are efficiency dips at 3.75 GHz

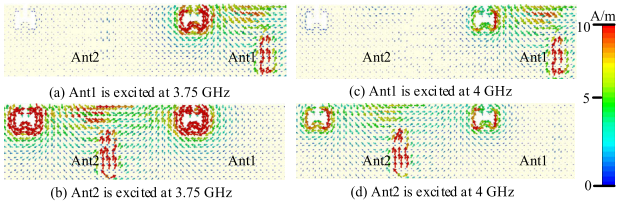

FIGURE 12. Surface current distributions around the slots in the ground.

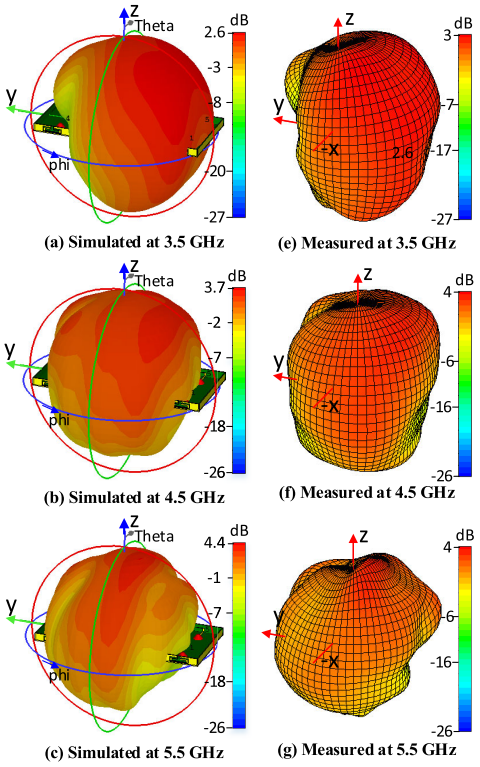

FIGURE 13. Simulated and measured 3-D radiation patterns of Ant 1 of the proposed MIMO antenna system.

in both Ant1 and Ant2 in Fig. 11(a). Then, we compared the current distribution around the decoupling-slot when Ant1 and Ant2 are excited separately at 3.75 GHz. We find that, when Ant1 is excited, the current only condenses in the decoupling-slot between Ant1 and Ant2. However, when Ant2 is excited there are strong current distribution around the two decoupling-slots adjacent to Ant2. As a result, the efficiency dip at 3.75 GHz of Ant2 is more than that of Ant1 in Fig. 11(a). Overall, the level of measured efficiency is higher than 40% across the target frequency bands.

B. MIMO PERFORMANCES

In this subsection, we investigated the envelope correlation coefficient (ECC) of proposed MIMO antenna system. ECC is a key factor to evaluate the diversity and multiplexing of a MIMO antenna system. Fig. 11(b) shows the simulated and calculated ECCs of antenna-pairs 1&2, 2&3, 1&5 and 2&6, respectively. We chose these antenna-pairs because they are close to each other and the radiation interference between

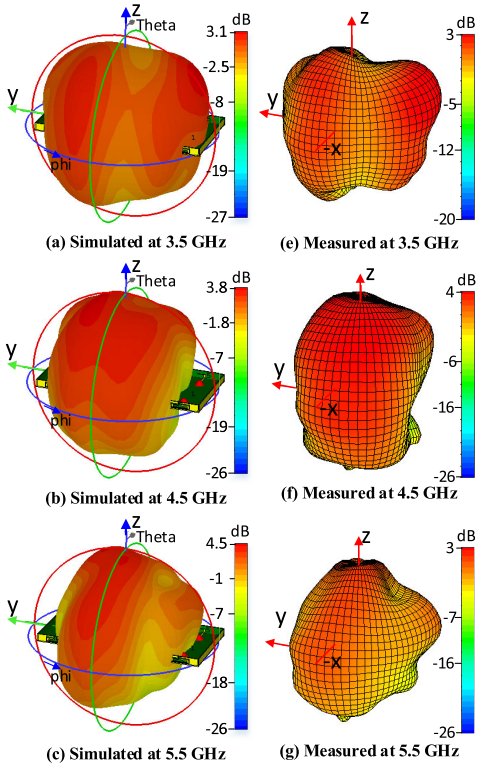

FIGURE 14. Simulated and measured 3-D radiation patterns of Ant2 of the proposed MIMO antenna system.

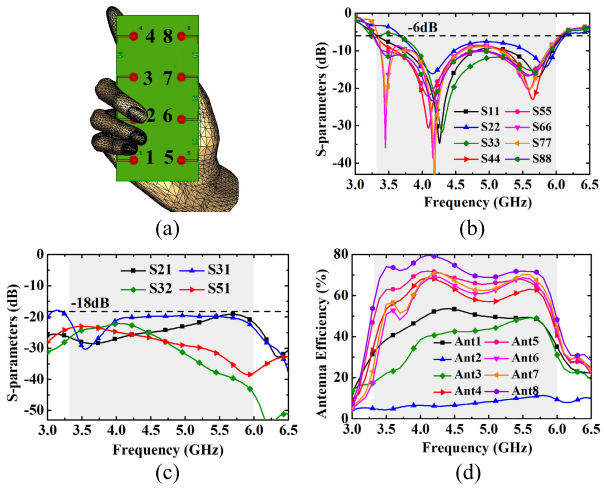

FIGURE 15. Simulated (b) reflection coefficients, (c) transmission coefficients and (d) antenna efficiencies of the MIMO antenna system with a single-hand model.

them are stronger than other pairs. What's more, the ECCs of the symmetrical antenna-pairs are not included here for brevity.

We calculated the ECC with the simulated and measured radiation far-field data from CST software and microwave anechoic chamber, respectively. In Fig. 11(b), the level of ECC is lower than 0.05 across the target frequency band, providing a promising MIMO diversity performance.

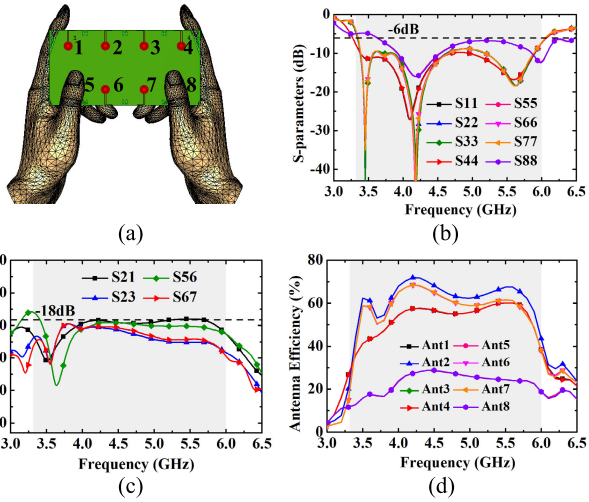

FIGURE 16. Simulated (b) reflection coefficients, (c) transmission coefficients and (d) antenna efficiencies of the MIMO antenna system with a double-hand model.

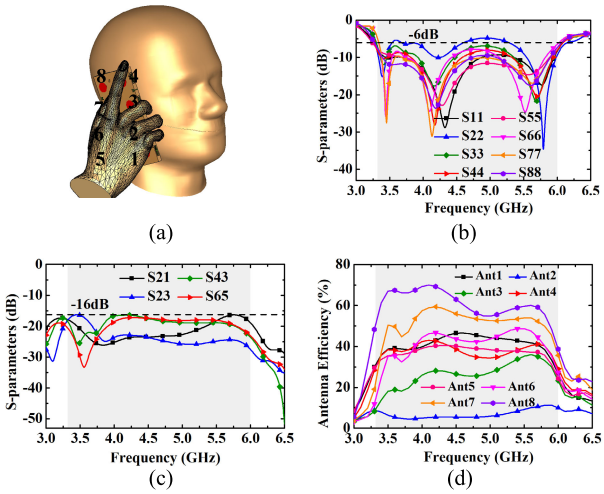

FIGURE 17. Simulated (b) reflection coefficients, (c) transmission coefficients and (d) antenna efficiencies of the MIMO antenna system with a head-hand model.

C. RADIATION PERFORMANCES

We analyzed the radiation patterns of Ant 1 and 2 in this subsection. Due to the symmetrical arrangement in MIMO antenna system, the radiation patterns of other antenna-elements are not included here for brevity.

The simulated and measured 3-D radiation patterns of Ant 1 and 2 at 3.5, 4.5 and 5.5 GHz are depicted in Fig. 13 and Fig. 14, respectively. The simulated and measured results match properly with each other. As in Fig. 13, the maximum radiation direction of Ant1 is tilted and pointed to the third quadrant at 3.5 GHz. At 4.5 and 5.5 GHz, the radiation patterns of Ant1 are also asymmetrical. The reason is that, the ground is asymmetrical for Ant1. In Fig. 14, the radiation patterns of Ant2 look more symmetrical than that of Ant1 across the frequency band. This is because that, the ground is relatively symmetrical for Ant2 compared with that for Ant1.

As a result, the maximum radiation directions of Ant1 and Ant2 are not pointing to each other across the frequency band, thus results in a decent ECC lower than 0.05. Additionally, the radiation performance is stable across the target frequency band.

D. USER'S HAND AND HEAD EFFECTS

Finally, we studied the effect of user's single-hand, double-hand and head-hand in this subsection. We analyzed the variation of reflection coefficients, transmission coefficients and radiation efficiencies in different situations, respectively.

In Fig. 15, the MIMO antenna system is simulated with a single-hand model. Although there is a slight deterioration of the impedance matching at the lower frequency band of Ant 2 and 3, the other antennas are still able to cover 3.3-6.0 GHz. The element-isolations remain higher than 18 dB. Due to the direct finger-touch of Ant 1-3, their radiation efficiencies decreased significantly, while the efficiencies of Ant 4-8 stay higher than 40% across the target frequency band.

In Fig. 16, the MIMO antenna system is simulated with a double-hand model. The Ant 5 and 8 are touched by the thumbs, thus results in degenerate impedance matching and radiation efficiency. Nonetheless, there are still six antenna-elements operating at 3.3-6.0 GHz with superior element-isolation over 18 dB and efficiency over 40%.

In Fig. 17, the MIMO antenna system is simulated with a head-hand model. The reflection coefficients remain stable and the level of element-isolation drops to 16 dB. In addition, the radiation efficiencies of some antennas decreased because the hand and head models absorbed a part of radiated energy. As a result, the efficiencies of Ant 2 and 3 are lower than 40%, the efficiencies of Ant 1, 4, 5 and 6 are around 40%, and the efficiencies of Ant 7 and 8 are still higher than 40%.

As a conclusion, the proposed MIMO antenna system can guarantee the robustness in practical applications.

IV. CONCLUSION

An ultra-wideband MIMO antenna system with high element-isolation in a metal-frame smartphone has been investigated in this paper. The MIMO antenna system has a bandwidth of 58%, an element-isolation level over 18 dB and a good radiating efficiency over 40% across the frequency band from 3.3 to 6.0 GHz. Besides, the stable and diverse radiation patterns can ensure the ECC level lower than 0.05. What's more, the performance remains decent under the effect caused by user's hands and head in the practical applications. Consequently, the proposed MIMO antenna system is a reliable candidate for 5G applications in mobile terminals.

REFERENCES

[1] J. G. Andrews, S. Buzzi, W. Choi, S. V. Hanly, A. Lozano, A. C. K. Soong, and J. C. Zhang, "What will 5G be?" *IEEE J. Sel. Areas Commun.*, vol. 32, no. 6, pp. 1065–1082, Jun. 2014.

[2] H. Li, X. Chen, and X. Zhou, "Cooperative management architecture and mechanism of 55 G-oriented distributed mobile cloud computing G-oriented," *ZTE Technol. J.*, vol. 21, no. 2, pp. 14–19, Feb. 2015.

[3] M. A. Jensen and J. W. Wallace, "A review of antennas and propagation for MIMO wireless communications," *IEEE Trans. Antennas Propag.*, vol. 52, no. 11, pp. 2810–2824, Nov. 2004.

[4] A. Al-Dulaimi, S. Al-Rubaye, Q. Ni, and E. Sousa, "5G communications race: Pursuit of more capacity triggers LTE in unlicensed band," *IEEE Veh. Technol. Mag.*, vol. 10, no. 1, pp. 43–51, Mar. 2015.

[5] M. Agiwal, A. Roy, and N. Saxena, "Next generation 5G wireless networks: A comprehensive survey," *IEEE Commun. Surveys Tuts.*, vol. 18, no. 3, pp. 1617–1655, 3rd Quart., 2016.

[6] A. Zhao and Z. Ren, "Size reduction of self-isolated MIMO antenna system for 5G mobile phone applications," *IEEE Antennas Wireless Propag. Lett.*, vol. 18, no. 1, pp. 152–156, Jan. 2019.

[7] H. Xu, H. Zhou, S. Gao, H. Wang, and Y. Cheng, "Multimode decoupling technique with independent tuning characteristic for mobile terminals," *IEEE Trans. Antennas Propag.*, vol. 65, no. 12, pp. 6739–6751, Dec. 2017.

[8] W. Jiang, B. Liu, Y. Cui, and W. Hu, "High-isolation eight-element MIMO array for 5G smartphone applications," *IEEE Access*, vol. 7, pp. 34104–34112, 2019.

[9] K.-L. Wong, J.-Y. Lu, L.-Y. Chen, W.-Y. Li, and Y.-L. Ban, "8-antenna and 16-antenna arrays using the quad-antenna linear array as a building block for the 3.5-GHz LTE MIMO operation in the smartphone," *Microw. Opt. Technol. Lett.*, vol. 58, no. 1, pp. 174–181, Jan. 2016.

[10] M.-Y. Li, Y.-L. Ban, Z.-Q. Xu, J. Guo, and Z.-F. Yu, "Tri-polarized 12-antenna MIMO array for future 5G smartphone applications," *IEEE Access*, vol. 6, pp. 6160–6170, 2018.

[11] X. Zhao, S. P. Yeo, and L. C. Ong, "Decoupling of inverted-F antennas with high-order modes of ground plane for 5G mobile MIMO platform," *IEEE Trans. Antennas Propag.*, vol. 66, no. 9, pp. 4485–4495, Sep. 2018.

[12] Y. Li, C.-Y.-D. Sim, Y. Luo, and G. Yang, "High-isolation 3.5 GHz eight-antenna MIMO array using balanced open-slot antenna element for 5G smartphones," *IEEE Trans. Antennas Propag.*, vol. 67, no. 6, pp. 3820–3830, Jun. 2019.

[13] N. O. Parchin, Y. I. A. Al-Yasir, A. H. Ali, I. Elfergani, J. M. Noras, J. Rodriguez, and R. A. Abd-Alhameed, "Eight-element dual-polarized MIMO slot antenna system for 5G smartphone applications," *IEEE Access*, vol. 7, pp. 15612–15622, 2019.

[14] Z. Ren, A. Zhao, and S. Wu, "MIMO antenna with compact decoupled antenna pairs for 5G mobile terminals," *IEEE Antennas Wireless Propag. Lett.*, vol. 18, no. 7, pp. 1367–1371, Jul. 2019.

[15] L. Sun, H. Feng, Y. Li, and Z. Zhang, "Compact 5G MIMO mobile phone antennas with tightly arranged orthogonal-mode pairs," *IEEE Trans. Antennas Propag.*, vol. 66, no. 11, pp. 6364–6369, Nov. 2018.

[16] M.-Y. Li, Z.-Q. Xu, Y.-L. Ban, C.-Y.-D. Sim, and Z.-F. Yu, "Eight-port orthogonally dual-polarised MIMO antennas using loop structures for 5G smartphone," *IET Microw., Antennas Propag.*, vol. 11, no. 12, pp. 1810–1816, Sep. 2017.

[17] M.-Y. Li, Y.-L. Ban, Z.-Q. Xu, G. Wu, C.-Y.-D. Sim, K. Kang, and Z.-F. Yu, "Eight-port orthogonally dual-polarized antenna array for 5G smartphone applications," *IEEE Trans. Antennas Propag.*, vol. 64, no. 9, pp. 3820–3830, Sep. 2016.

[18] K.-L. Wong, C.-Y. Tsai, and J.-Y. Lu, "Two asymmetrically mirrored gap-coupled loop antennas as a compact building block for eight-antenna MIMO array in the future smartphone," *IEEE Trans. Antennas Propag.*, vol. 65, no. 4, pp. 1765–1778, Apr. 2017.

[19] Y. Liu, A. Ren, H. Liu, H. Wang, and C.-Y.-D. Sim, "Eight-port MIMO array using characteristic mode theory for 5G smartphone applications," *IEEE Access*, vol. 7, pp. 45679–45692, 2019.

[20] L. Chang, Y. Yu, K. Wei, and H. Wang, "Polarization-orthogonal co-frequency dual antenna pair suitable for 5G MIMO smartphone with metallic bezels," *IEEE Trans. Antennas Propag.*, vol. 67, no. 8, pp. 5212–5220, Aug. 2019.

[21] Y. Li, C.-Y.-D. Sim, Y. Luo, and G. Yang, "Multiband 10-antenna array for sub-6 GHz MIMO applications in 5-G smartphones," *IEEE Access*, vol. 6, pp. 28041–28053, 2018.

[22] Y. Li, C.-Y.-D. Sim, Y. Luo, and G. Yang, "12-port 5G massive MIMO antenna array in sub-6 GHz mobile handset for LTE bands 42/43/46 applications," *IEEE Access*, vol. 6, pp. 344–354, 2018.

[23] Z. Ren and A. Zhao, "Dual-band MIMO antenna with compact self-decoupled antenna pairs for 5G mobile applications," *IEEE Access*, vol. 7, pp. 82288–82296, 2019.

[24] J. Guo, L. Cui, C. Li, and B. Sun, "Side-edge frame printed eight-port dual-band antenna array for 5G smartphone applications," *IEEE Trans. Antennas Propag.*, vol. 66, no. 12, pp. 7412–7417, Dec. 2018.

[25] J. Li, X. Zhang, Z. Wang, X. Chen, J. Chen, Y. Li, and A. Zhang, "Dual-band eight-antenna array design for MIMO applications in 5G mobile terminals," *IEEE Access*, vol. 7, pp. 71636–71644, 2019.

[26] Y.-L. Ban, C. Li, C.-Y.-D. Sim, G. Wu, and K.-L. Wong, "4G/5G multiple antennas for future multi-mode smartphone applications," *IEEE Access*, vol. 4, pp. 2981–2988, 2016.

[27] W. Jiang, Y. Cui, B. Liu, W. Hu, and Y. Xi, "A dual-band MIMO antenna with enhanced isolation for 5G smartphone applications," *IEEE Access*, vol. 7, pp. 112554–112563, 2019.

[28] W. Hu, L. Qian, S. Gao, L.-H. Wen, Q. Luo, H. Xu, X. Liu, Y. Liu, and W. Wang, "Dual-band eight-element MIMO array using multi-slot decoupling technique for 5G terminals," *IEEE Access*, vol. 7, pp. 153910–153920, 2019.

[29] A. Zhao and Z. Ren, "Wideband MIMO antenna systems based on coupled-loop antenna for 5G N77/N78/N79 applications in mobile terminals," *IEEE Access*, vol. 7, pp. 93761–93771, 2019.

[30] Q. Chen, H. Lin, J. Wang, L. Ge, Y. Li, T. Pei, and C.-Y.-D. Sim, "Single ring slot-based antennas for metal-rimmed 4G/5G smartphones," *IEEE Trans. Antennas Propag.*, vol. 67, no. 3, pp. 1476–1487, Mar. 2019.

[31] X. Zhang, Y. Li, W. Wang, and W. Shen, "Ultra-wideband 8-Port MIMO antenna array for 5G metal-frame smartphones," *IEEE Access*, vol. 7, pp. 72273–72282, 2019.

[32] S. H. Chae, S.-K. Oh, and S.-O. Park, "Analysis of mutual coupling, correlations, and TARC in WiBro MIMO array antenna," *IEEE Antennas Wireless Propag. Lett.*, vol. 6, pp. 122–125, 2007.

[33] C. F. Ding, X. Y. Zhang, C.-D. Xue, and C.-Y.-D. Sim, "Novel pattern-diversity-based decoupling method and its application to multielement MIMO antenna," *IEEE Trans. Antennas Propag.*, vol. 66, no. 10, pp. 4976–4985, Oct. 2018.

[34] T. S. P. See and Z. N. Chen, "An ultrawideband diversity antenna," *IEEE Trans. Antennas Propag.*, vol. 57, no. 6, pp. 1597–1605, Jun. 2009.

[35] M. S. Khan, A.-D. Capobianco, B. D. Braaten, A. Naqvi, B. Ijaz, and S. Asif, "Planar, compact ultra-wideband polarisation diversity antenna array," *IET Microw., Antennas Propag.*, vol. 9, no. 15, pp. 1761–1768, Dec. 2015.

[36] C.-C. Hsu, K.-H. Lin, and H.-L. Su, "Implementation of broadband isolator using metamaterial-inspired resonators and a T-Shaped branch for MIMO antennas," *IEEE Trans. Antennas Propag.*, vol. 59, no. 10, pp. 3936–3939, Oct. 2011.

[37] A. B. Numan, M. S. Sharawi, A. Steffes, and D. N. Aloi, "A defected ground structure for isolation enhancement in a printed MIMO antenna system," in *Proc. 7th Eur. Conf. Antenna Propag. (EUCAP)*, Gothenburg, Sweden, Apr. 2013, pp. 2123–2126.

[38] S. R. Thummaluru, R. Kumar, and R. K. Chaudhary, "Isolation enhancement and radar cross section reduction of MIMO antenna with frequency selective surface," *IEEE Trans. Antennas Propag.*, vol. 66, no. 3, pp. 1595–1600, Mar. 2018.

[39] H.-J. Jiang, Y.-C. Kao, and K.-L. Wong, "High-isolation WLAN MIMO laptop computer antenna array," in *Proc. Asia–Pacific Microw. Conf. Proc.*, Kaohsiung City, Taiwan, Dec. 2012, pp. 319–321.

[40] J. Deng, J. Li, L. Zhao, and L. Guo, "A dual-band inverted-F MIMO antenna with enhanced isolation for WLAN applications," *IEEE Antennas Wireless Propag. Lett.*, vol. 16, pp. 2270–2273, 2017.

[41] C.-H. Wu, G.-T. Zhou, Y.-L. Wu, and T.-G. Ma, "Stub-loaded reactive decoupling network for two-element array using even–odd analysis," *IEEE Antennas Wireless Propag. Lett.*, vol. 12, pp. 452–455, 2013.

[42] L. Chang, Y. Yu, K. Wei, and H. Wang, "Orthogonally-polarized dual antenna pair with high isolation and balanced high performance for 5G MIMO smartphone," *IEEE Trans. Antennas Propag.*, early access, Jan. 9, 2020, doi: 10.1109/TAP.2020.2963918.

[43] L. Sun, Y. Li, Z. Zhang, and Z. Feng, "Wideband 5G MIMO antenna with integrated orthogonal-mode dual-antenna pairs for metal-rimmed smartphones," *IEEE Trans. Antennas Propag.*, early access, Oct. 28, 2019, doi: 10.1109/TAP.2019.2948707.

XIAO-TING YUAN received the B.E. degree from Huaqiao University, Fujian, China. She is currently pursuing the master's degree in information and communication engineering with Shenzhen University, Shenzhen, China. Her current research interest includes the development and application of mobile terminal antennas.

WEI HE received the B.E. degree from Xidian University, Xi'an, Shaanxi, China. He is currently an Engineer with the China Academy of Information and Communications Technology. His current research interest includes the development and application of mobile terminal antennas.

KAI-DONG HONG received the B.E. degree in communication engineering from Guangdong Ocean University, Zhanjiang, Guangdong, China. He is currently pursuing the Ph.D. degree in information and communication engineering with Shenzhen University, Shenzhen, Guangdong. His current research interests include planar microwave and millimeter-wave antennas and smart antennas for mobile terminals.

CHONG-ZHI HAN received the B.E. and M.E. degrees in electronic information engineering from the Harbin Institute of Technology (HIT), Harbin, China. He is currently pursuing the Ph.D. degree in information and communication engineering with Shenzhen University, Shenzhen, China. His current research interests include the development and application of MIMO antennas and millimeter wave antenna.

ZHE CHEN (Member, IEEE) received the B.E. degree in electronic information engineering and the M.E. degree in electronics and telecommunications engineering from Xidian University, Xi'an, Shaanxi, China, in 2012 and 2015, respectively, and the Ph.D. degree in electronic engineering from the City University of Hong Kong, Hong Kong, in 2018.

He was a Postdoctoral Fellow with the State Key Laboratory of Terahertz and Millimeter Waves, City University of Hong Kong, from 2018 to 2019. He was a Research Assistant with the Information and Communication Technology Centre, Shenzhen Research Institute, City University of Hong Kong, in 2015. He is currently an Assistant Professor with the College of Electronics and Information Engineering, Shenzhen University, Shenzhen, Guangdong, China. His research interests include reconfigurable antennas, dielectric resonator antennas, millimeter wave antennas, antennas for mobile terminals and 5G applications, and so on. He was a TPC Member of the IWEM 2019.

TAO YUAN (Member, IEEE) received the B.E. degree in electronic engineering and the M.E. degree in signal and information processing from Xidian University, Xi'an, Shaanxi, China, in 1999 and 2003, respectively, and the Ph.D. degree in electrical and computer engineering from the National University of Singapore, Singapore, in 2009.

He was a Visiting Scholar with the University of Houston, from 2007 to 2008, and a Research and Development Manager of Antenna with Molex, LLC, USA, and Hi-P International Ltd., Singapore, from 2008 to 2012. Since 2016, he has been a Distinguished Professor with the ATR National Key Laboratory of Defense Technology, College of Electronics and Information Engineering, Shenzhen University, Shenzhen, Guangdong, China, where he is currently the Director of the Guangdong Provincial Mobile Terminal Microwave and Millimeter-Wave Antenna Engineering Research Center. His current research interests include the development of novel RF modules and antennas for mobile terminals and 5G applications.

Dr. Yuan is a member of the IEEE Antennas and Propagation Society, the IEEE Microwave Theory and Techniques Society, and the China Communications Standards Association.